THE INFLUENCE OF WELDING TIME ON MECHANICAL PROPERTIES OF RESISTANCE SPOT WELDED TWIP STEEL SHEETS

Hakan AYDIN[1], Mumin TUTAR[1], Ali BAYRAM[1]
Uludag University, Engineering Faculty, Mechanical Engineering Department, Turkey[1]
hakanay@uludag.edu.tr

Abstract: *This paper presents an analysis of the welding time effect on the mechanical properties of resistance spot welded TWIP980 steel sheets. Optical microscopy, microhardness measurements across the welded joints, and tensile shear tests of the joints were conducted to evaluate the quality of the joints. With welding time increasing, a macro expulsion cavity occurred in the FZ. The NS increased with increasing welding time up to 300 ms, and above 300 ms it decreased. On the other hand, the indentation depth increased almost linearly with increasing welding time. The hardness values in FZ and HAZ were lower than that in the BM. The lowest hardness values were observed in the HAZ. However, higher welding time led to higher hardness in HAZ. The tensile shear load, tensile shear deformation and failure energy of the joints increased with increasing welding time, but above 300 or 350 ms, these values decreased.*

Keywords: TWIP STEEL; RESISTANCE SPOT WELDING; WELDING TIME; MECHANICAL PROPERTIES.

1. Introduction

Innovative TWinning-Induced Plasticity (TWIP) steels are frequently used for car body manufacturing to reduce the vehicles weight and to improve passenger safety. TWIP steels, which have a fully austenitic microstructure due to their high manganese content of 17% to 24% and a significant percentage of carbon, have highly desirable mechanical properties exhibiting both high strength and large ductility in a sheet forming[1]. The deformation mechanism of the TWIP steel involves twinning as well as dislocation slip[2,3].

The use of metal sheets in the automotive applications inevitably involves welding[4]. Resistance spot welding (RSW) is an effective way to join metal sheets. However, important changes occur in mechanical and metallurgical properties of the spot welded area and heat affected zone (HAZ) during the RSW process due to the welding thermal cycle[5]. In the previous studies concerning the RSWed TWIP steels, Razmpoosh et al.[6] investigated the resistance spot weldability of a Fe–31Mn–3Al–3Si TWIP steel and reported that due to the expulsion phenomenon, optimum welding parameters for the experimental TWIP steel were shifted to lower values. Spena et al.[7] studied on dissimilar resistance spot welding of TWIP and Quenching and Partitioning (Q&P) steel grades and stated that the weld spots predominantly failed at the TWIP side. Spena et al.[8] also examined the effects of the main important process parameters on the mechanical and microstructural properties of resistance spot welded TWIP sheets and reported that the tensile shear samples mainly failed by interfacial fracture mode, while partial thickness with pull out fractures were observed in the samples when a high welding current and clamping force were used. Ashiri et al.[9] studied on liquid metal embrittlement of Zn-coated TWIP steel welds and obtained liquid metal embrittlement-free welds which is able to extend the weldable current range of TWIP steels. Saha et al. [10] investigated the HAZ liquation crack and segregation behavior of the resistance spot welded TWIP steel and reported that cracks had less/no significant effect on the static cross-tensile strength (CTS) and the tensile-shear strength (TSS). Yu et al. [11] studied on improvement of weldability of 1 GPa grade TWIP Steel and found that larger nugget size (NS) and higher tensile shear strength were obtained in constant power control welding than constant current control welding.

It is important to study the welding behavior of the resistance spot-welded joints of TWIP sheet steels since these steels are gaining popularity in the modern automotive applications. The aim of the present research is investigating the microstructural and mechanical properties of resistance spot welded TWIP980 steel at different welding time.

2. Materials and Procedures

In this study, high-Mn (TWIP980) steel of 1.3 mm thickness was used. This steel has the following composition (wt.%): C, 0.28; Mn, 15.6; Si, 1.06; Al, 1.89; Cr, 0.564; Ti, 0.1; and Fe, balance. The 0.2% proof strength, ultimate tensile strength and elongation of TWIP980 steel used in this investigation are 640 MPa, 982 MPa and 46%, respectively. The bulk specimens were cut into sample for tensile-shear test using laser cutting machine with the dimensions 50 mm x 20 mm.

The specimens were cleaned properly with ethanol to remove dirt, oil, oxide and surface scale before welding. Welding was performed by overlapping the sheets using MFDC resistance spot-welding machine connected to ABB robot arm (Fig.1). Cu alloy electrodes with tip diameter of 6 mm were used. The spot welds were performed with welding times of 200 ms, 250 ms, 300 ms, 350 ms and 400 ms while keeping the weld current and electrode force constant at 12 kA and 3 kN, respectively.

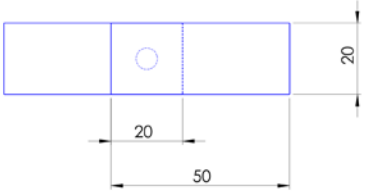

Fig.1 The welded tensile shear test sample.

The spot welded joints were cross sectioned through the weld nugget center using an electrical-discharge cutting machine. The microstructure was revealed using both Nital (%3) and $Na_2S_2O_5$ solution (10 g $Na_2S_2O_5$ in 100 ml H_2O), respectively. The optical microscopic studies were carried out by a Nikon DIC microscope under polarized light with a Clemex image analysis system. The NS of the welds was measured through the fractured specimens using Mitutoyo digital caliper. The Vickers microhardness measurement was carried out with a load of 200 g for HAZ and base metal (BM) and 500 g for fusion zone (FZ) due to the coarse dendritic structure in FZ, and loading time 10 s. The tensile shear tests were performed with a fully computerized UTEST-7014 tensile testing machine using a constant strain rate of $3.33x10^{-3}$ s^{-1}.

3. Results and Discussion

Optical microscope was used to analyze the microstructural changes (Fig.2). There is typically one phase present in the microstructure of TWIP steels, face centered cubic (fcc). Fig. 2a shows that the microstructure in the BM mainly consists of fine grained austenite including mechanical twins, with evident bands in the rolling directions. Austenite becomes significant larger in the HAZ than in the BM, as seen in Fig. 2b. This is due to the grain growth was not restricted by the formation of any phases, such as ferrite and martensite, during thermal cycles. The FZ is full of a columnar dendritic austenitic microstructure (cast microstructure), as shown in Fig. 2c.

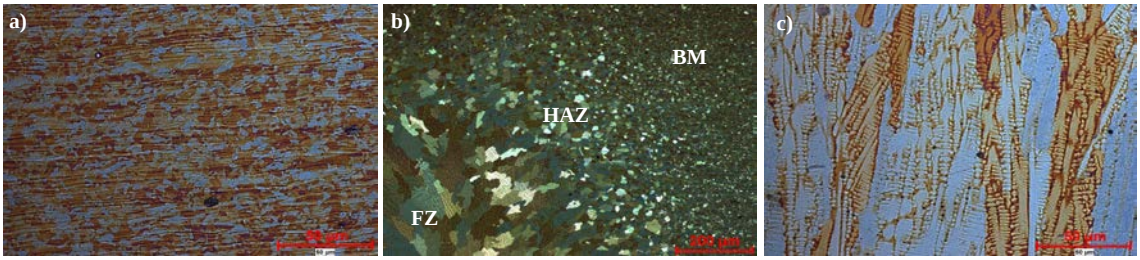

Fig.2 Microstructural changes from the BM to the FZ via optical microscopy observations. (a) BM, (b) transition zone between FZ and BM, (c) FZ. (The joint with welding time of 300 ms).

Interdendritic micro-pores formed as a consequence of solidification shrinkage could be observed in FZ of all samples, as shown in Fig.3. On the other hand, a macro expulsion cavity in FZ were not seen in all samples (Fig.4). This macro cavity results from the molten material loss in the FZ with the expulsion phenomenon during RSW process. In this context, the spot welds made with the higher welding time (the extensive expulsion phenomenon with the higher heat input) exhibited more commonly this macro expulsion cavity in FZ than those made with the lower welding time (Fig.4).

The NS increased with an increase of welding time up to 300 ms, as shown in Fig. 5a. When the welding time reached 350 ms, the NS of the spot welded joint dropped instead owing to the excessive expulsion. On the other hand, the indentation depth of the spot welded joints increased almost linearly with increasing welding time owing to the enhanced expulsion phenomenon during RSW process with higher heat input (Fig.5b).

Fig.3 Interdendritic micro-pores in FZ. (The joint with welding time of 300 ms).

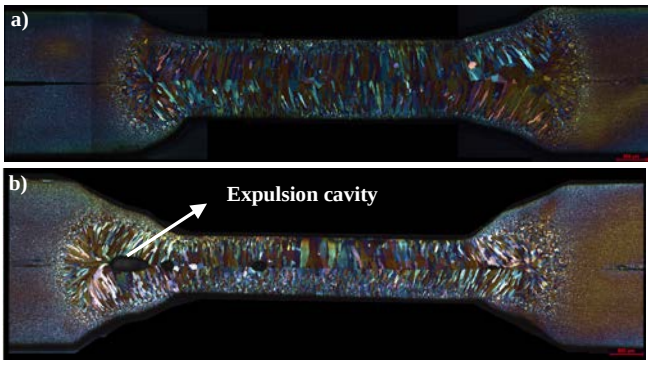

Fig.4 The effect of welding time on the formation of a expulsion cavity: a) 250 ms, b) 350 ms.

The microhardness was measured on the FZ, HAZ and BM as shown in Fig. 6a, which was performed on a vickers hardness measurement device. BM hardness of TWIP980 steel sheets was about 260 $HV_{0.2}$. It can be seen that the microhardness of FZ and HAZ for all joints was always lower than that of BM. The softening in the weld zone (FZ and HAZ) can be attributed to the significantly larger grains in the weld zone, segregation of the alloying elements in these zones and lower carbon percentage in the FZ due to the decarburization during RSW process[12-14]. HAZs of the joints had the lowest hardness values, which increased with welding time. However, any relationship between the hardness values in FZ and welding time was not obtained.

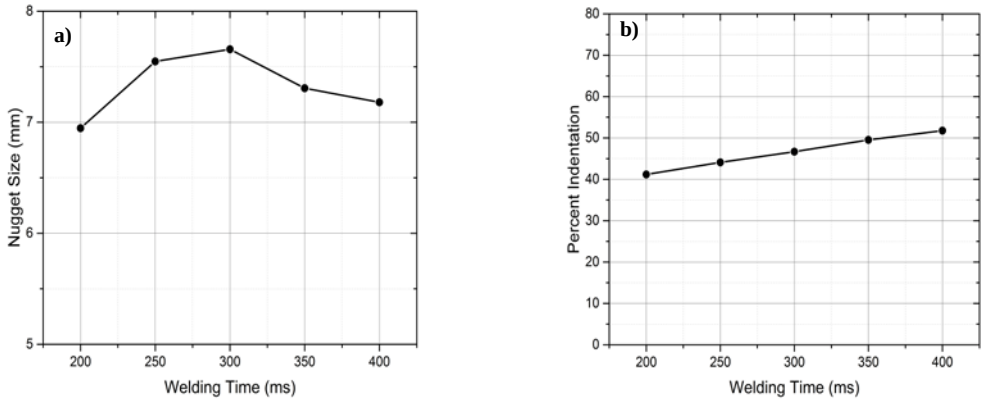

Fig.5 NS (a) and indentation depth (b) of the resistance spot-welded TWIP joints versus welding time.

In the tensile shear tests, all resistance spot-welded TWIP joints exhibited a full button pull-out failure mode referring to higher deformation energy, in which fracture occurs in the HAZ at the around of the spot weld. The effect of welding time on the tensile shear load, tensile shear deformation and failure energy absorption capacity of the spot welded joints is shown in Fig. 6b. The tensile shear load increased with an increasing of the welding time at initial stage and reached the maximum value at the range of 250-300 ms of welding time. This increase could be attributed to the increase of the NS owing to the higher heat input with increasing of welding time. Then, with an increasing of welding time from 300 ms to 400 ms, the tensile shear load of the spot-welded joints decreased almost linearly (Fig. 6b). This decrease could be associated with the decrease of NS and increase of the indentation depth with excessive expulsion due to the overheating of welding zone with increasing welding time[15]. The tensile shear deformations of the spot welded joints increased with increasing welding time up to 350 ms (Fig. 6b). Then, the tensile shear deformation dramatically decreased at the welding time of 400 ms owing to the decrease of NS and increase of the indentation depth. The failure energy absorption capacity of the spot welded joints was determined as the area under the tensile-deformation curve up to the peak load (Fig. 7). The failure energy increased with increasing welding time up to 300 ms, and then it decreased with increasing welding time (Fig. 6b). This behavior is more consistent with the tensile shear loads than the tensile deformation values of the joints. The results suggested that the welding time has an obvious effect on the tensile shear load bearing capacity and failure energy absorption of the spot welded joint

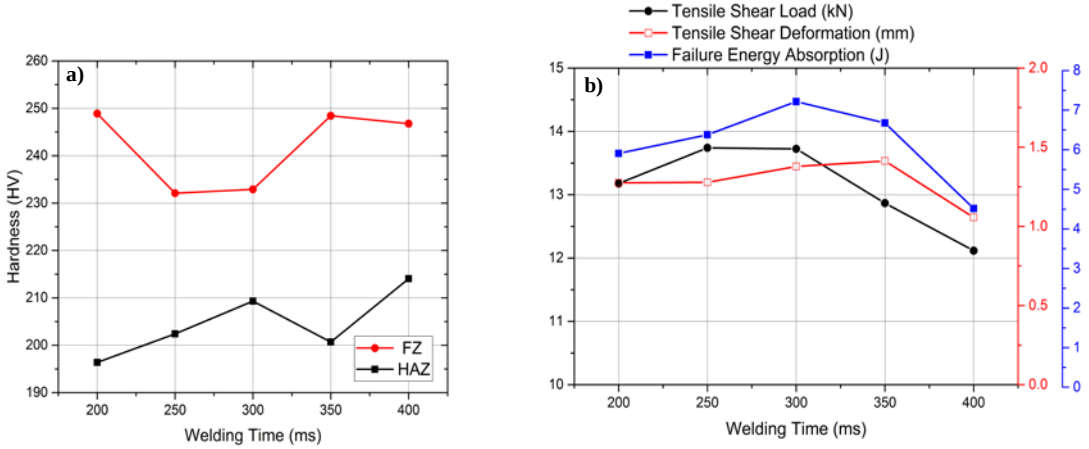

Fig.6 The effect of welding time on the hardness of welding zone (a) and on the tensile shear properties and failure energy absorption capacity of the resistance spot-welded TWIP980 joints.

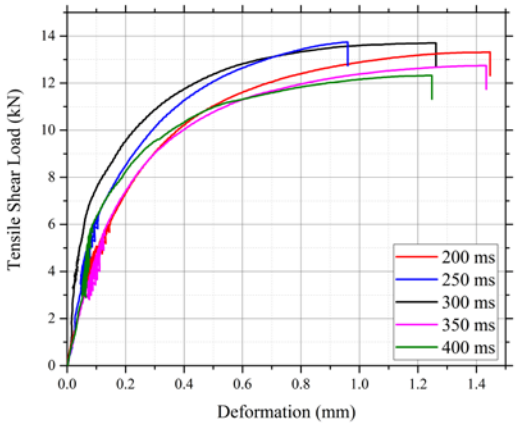

Fig.7 Tensile shear curves of the resistance spot-welded TWIP980 joints with different welding time.

4. Conclusions

The conclusions derived from this study can be given as follows:

- Higher welding time could lead to the formation of a macro expulsion cavity in FZ.
- Up to 300 ms, the NS of the spot welded joints increases with an increase of welding time. Above 300 ms, the NS decreases with increasing of welding time.
- The indentation depth of the spot welded joints increases almost linearly with increasing welding time.
- The hardness in the weld zone (FZ and HAZ) of the resistance spot welded TWIP980 steel sheets is lower than that of BM. HAZ of the joints had the lowest hardness and HAZ hardness relatively increases with increasing of welding time. However, there is not any relationship between the hardness values in FZ and welding time.
- The maximum joint strength is at the welding time of 250 ms and 300 ms. Above 300 ms, the joint strength decreases almost linearly with an increase of welding time.
- The tensile-shear deformation increases with increasing welding time of up to 350 ms. But, the tensile shear deformation dramatically decreases at the welding time of 400 ms.
- The failure energy increases with increasing welding time up to 300 ms, and above 300 ms, it decreases with increasing welding time.

ACKNOWLEDGMENTS

The authors are grateful to the Scientific and Technological Research Council of Turkey (TUBITAK) for its financial support to this research (Project number: MAG 213M597). The authors are also grateful to Ermetal Inc. for providing facilities for the resistance spot-welding processes.

References

1. R.W. Neu. Performance and characterization of TWIP steels for automotive applications. Materials Performance and Characterization 2(1) (2013) 244-284.
2. O. Grassel, L. Kruger, G. Frommeyer, L.W. Meyer. High strength Fe–Mn–(Al, Si) TRIP/TWIP steels: development, properties, and application. International Journal of Plasticity 16 (2000), 1391-1409.
3. K. Chung, K. Ahn, D.-H. Yoo, K.-H. Chung, M.-H. Seo, S.-H. Park. Formability of TWIP (twinning induced plasticity) automotive sheets. International Journal of Plasticity 27(1) (2011), 52–81.
4. Aydin H. The mechanical properties of dissimilar resistance spot welded DP600-DP1000 steel joints for automotive applications. Proceedings of the Institution of Mechanical Engineers, Part D: Journal of Automobile Engineering 229(5) (2015), 599-610.
5. M. Vural, A. Akkuş. On the resistance spot weldability of galvanized interstitial free steel sheets with austenitic stainless steel sheets. Journal of Materials Processing Technology 153-154 (2004), 1-6.
6. M.H. Razmpoosh, M. Shamanian, M. Esmailzadeh. The microstructural evolution and mechanical properties of resistance spot welded Fe–31Mn–3Al–3Si TWIP steel. Materials & Design 67 (2015), 571-576.
7. P.S. Spena, M. De Maddis, F. Lombardi, M. Rossini. Dissimilar resistance spot welding of Q&P and TWIP steel sheets. Materials and Manufacturing Processes 31(3) (2016) 291-299.
8. P.S. Spena, M. De Maddis, F. Lombardi, M. Rossini. Investigation on resistance spot welding of TWIP steel sheets. Steel Research International 86(12) (2015) 1480-1489.
9. R. Ashiri, M. Shamanian, H.R. Salimijazi, M.A. Haque, J.-H. Bae, C.-W. Ji, K.-G. Chin, Y.-D. Park. Liquid metal embrittlement-free welds of Zn-coated twinning induced plasticity steels. Scripta Materialia 114 (2016) 41-47.
10. D.C. Saha, I.S. Chang, Y.-D. Park. Heat-affected zone liquation crack on resistance spot welded TWIP steels. Materials Characterization, 93 (2014), 40-51.
11. J. Yu, D. Choi, S. Rhee. Improvement of weldability of 1 GPa grade Twin-Induced Plasticity Steel. Welding Journal 93 (2014) 78-84.
12. D. C. Saha, Y. Cho and Y.-D. Park. Metallographic and fracture characteristics of resistance spot welded TWIP steels. Science and Technology of Welding and Joining 18(8) (2013) 711-720.
13. D.C. Saha, S. Han, K.G. Chin, I.D. Choi, Y.D. Park. Weldability Evaluation and Microstructure Analysis of Resistance-Spot-Welded High-Mn Steel in Automotive Application. Steel Research International 83(4) (2012) 352-357.
14. M. Pouranvari, S. Marashi. Critical review of automotive steels spot welding: process, structure and properties. Science and Technology of Welding and Joining 18 (2013), 391-403.
15. N. Akkas and E. Ilhan. Effect of welding current on mechanical properties of welding joints in SPA-C steel sheets in resistance spot welding. Acta Physica Polinica A 125(2) (2014) 497-499.